PLEKHA7, an apical adherens junction protein, suppresses inflammatory breast cancer in the context of high E-cadherin and p120-catenin expression.

Lindy J Pence
Mayo Clinic
Antonis Kourtidis
Medical University of South Carolina
Ryan W. Feathers
Mayo Clinic
Mary T. Haddad
Mayo Clinic
Sotiris Sotiriou
Mayo Clinic
Paul Decker
Mayo Clinic
Aziza Nassar
Mayo Clinic
Idris T. Ocal
Mayo Clinic
Sejal S. Shah
Kaiser Permanente
Panos Z Anastasiadis (panos@mayo.edu)
Mayo Clinic Cancer Center https://orcid.org/0000-0003-4436-9435

Research article

Keywords: Inflammatory breast cancer, PLEKHA7, adherens junction, cadherin-catenin complexes

Posted Date: August 12th, 2020

DOI: https://doi.org/10.21203/rs.3.rs-57687/v1

Version of Record: A version of this preprint was published at International Journal of Molecular Sciences on January 28th, 2021. See the published version at https://doi.org/10.3390/ijms22031275.

Abstract

Background: Inflammatory breast cancer is a highly aggressive form of breast cancer that robustly forms clusters of tumor emboli in dermal lymphatics and readily metastasizes. Inflammatory breast cancers express high levels of E-cadherin, the major protein of adherens junctions, which may enhance the ability of tumor cells to form such clusters and contribute to metastasis. Seemingly contradictory, E-cadherin has both tumor-suppressing and tumor-promoting roles in cancer; previous studies suggest that this depends on the balance between apical and basolateral cadherin-catenin complexes.

Methods: In the present study, we use immunohistochemistry of inflammatory breast cancer patient samples and biochemical analysis of cell lines to determine the expression of PLEKHA7, an apical adherens junction protein. We use viral transduction to ectopically express PLEKHA7 in the SUM149 inflammatory breast cancer cell line. The effect of PLEKHA7 on the aggressiveness of inflammatory breast cancer in 2D, 3D and in-vivo were examined.

Results: We determined that PLEKHA7 was deregulated in inflammatory breast cancer, demonstrating improper localization or lost expression in a strong majority of patient samples and very low expression in cell line models. We found that re-expressing PLEKHA7 is sufficient to suppress proliferation, anchorage independent growth, spheroid viability, and tumor growth in-vivo. We also observed a negative-selection pressure within the xenograft tumors to lose PLEKHA7 function or expression.

Conclusions: The data indicate that PLEKHA7 is frequently deregulated and acts as a suppressor of inflammatory breast cancer. They also suggest that the resulting imbalance between apical and basolateral cadherin-catenin complexes contributes to growth, survival and emboli-forming capacities of inflammatory breast cancer.

Introduction

Inflammatory breast cancer (IBC) is an aggressive subset of breast cancer, comprising approximately 2% of breast cancer diagnoses in the US (1) (2). Yet, mortality from IBC is disproportionately responsible for around 7% of deaths from breast cancer each year (1). IBC requires both a clinical and pathologic diagnosis. Patients develop rapid onset (< 6 months) redness, painful swelling and dimpling of the skin, referred to as “peau-de-orange” because the skin resembles that of an orange peel, encompassing at least 1/3 of the breast. In addition to this clinical picture, IBC requires pathologic diagnosis of invasive carcinoma (3). Dermal biopsy frequently reveals the presence of “tumor emboli” in the dermal lymphatics. The characteristic tumor emboli are considered responsible for the clinical phenotype of IBC patients, as these emboli may clog the lymphatic drainage system.

Extensive work has been done to profile IBC patient samples by RNA and genetics in order to understand the differences between IBC and non-IBC. This has proved quite challenging (see (4) for review). However, over 20 years ago, it was observed that IBC patients and IBC models express disproportionately high levels of the adherens junction (AJ) protein E-cadherin (5–7). Targeting E-cadherin with function-blocking

antibodies in the MARY-X animal model of IBC led to a dramatic reduction in the number and size of tumor emboli (7). It is expected that E-cadherin maintains adhesion between tumor cells within the emboli to facilitate safe and effective passage through the lymphatics. The viability of tumor emboli within circulatory systems likely contributes to high rates of metastasis in IBC.

E-cadherin mediates epithelial cell-cell adhesion via trans homophilic interaction with E-cadherin of neighboring cells. It binds several catenin-family members via its cytoplasmic domain and is linked to the actin and microtubule cytoskeleton through these interactions (8). E-cadherin is regularly turned over via endosome-lysosomal sorting, but this turnover is inhibited by E-cadherin interaction with p120-catenin (p120) (9–11). p120 binds the cytoplasmic juxtamembrane region of E-cadherin and protects E-cadherin from cleavage, clathrin-mediated endocytosis, or ubiquitination by Hakai (12–16). Not surprisingly, p120 is also required for IBC tumor growth and emboli formation. p120 expression is increased in IBC through internal ribosomal entry site (IRES)-mediated translation via the translation initiation factor eIF4GI, which is overexpressed in approximately 80% of IBC patient samples (17).

The cadherin-catenin complexes localize at the apical AJs and also along basolateral contacts (18). Recent work from our lab determined that the basolateral complexes promote tumor progression via increased expression of Cyclin D1, Snail, and Myc and also increased Src family kinase activity (19). However, apical cadherin-catenin complexes suppress the translation of these proteins through the function of PLEKHA7, an apical AJ-specific interacting partner of p120 (19–21). PLEKHA7 recruits the micro-RNA (miRNA) processing machinery to the apical AJs, promotes the generation of mature miRNAs, and facilitates loading of miRNAs onto a junctional RNA-induced silencing complex (RISC), resulting in local suppression of mRNA translation (19, 22). Loss of PLEKHA7-mediated RNA interference (RNAi) at the apical AJs leads to higher expression of Cyclin D1, Snail and Myc and results in gain of anchorage independent growth (AIG) in colon epithelial cells (19).

Given that IBC patients express high levels of E-cadherin and p120, we hypothesize that an imbalance of the pro-growth basolateral cadherin-catenin complexes and tumor-suppressing apical AJs contributes to the pathophysiology of IBC. In this study, we look at PLEKHA7 expression and function in IBC models. We find that patients and cell models largely lack functional PLEKHA7. When PLEKHA7 is restored in cell and xenograft models, we find that the aggressive nature of IBC is mitigated. Our results provide insight into the nuances of the cadherin-catenin axis' contribution to IBC and suggest that PLEKHA7 acts as a suppressor of IBC.

Materials And Methods

Constructs:

The full length human PLEKHA7 construct utilized in this study was previously described (19). The LZRS-ms neo plasmid was a generous gift from Dr. Albert Reynolds (Vanderbilt University). TopFlash and FopFlash reporter plasmids were a kind gift from Dr. Aubrey Thompson (Mayo Clinic Florida) and were

originally acquired from Upstate Cell Signaling Solutions (21–170 and 21–169). Renilla-TK plasmid (pGL4.74, hRluc/TK) was purchased from Promega (E6921).

Immunofluorescence:

Cells were grown to confluence on glass coverslips and fixed by either 100% methanol or 4% paraformaldehyde/4% sucrose. Coverslips were rinsed with PBS and cells fixed with methanol in -20 °C for 7 minutes. Alternatively, coverslips were rinsed with PBS, fixed in paraformaldehyde at room temperature for 15 minutes, washed twice with PBS/10 mM glycine for 5 minutes each, and solubilized with PBS containing 0.2% Triton X-100 for 5 minutes. Coverslips were blocked with Dako protein block (Agilent) and incubated with primary antibody diluted in Dako antibody diluent (Agilent) overnight. Coverslips were washed three times in PBS, exposed to secondary antibodies for 1 hour, washed once in PBS, washed in PBS + 4, 6-Diamidino-2-phenylindole dihydrochloride (DAPI) (Sigma, D8417) to stain nuclei, followed by two additional PBS washes. Coverslips were then mounted on glass slides with Aqua Poly/Mount (Polysciences) and imaged using a 63X oil objective on a Carl Zeiss LSM 800 confocal microscope. Z-stacks were taken using 0.5 µm intervals. All image processing, including generation of maximum projection intensity images and addition of scale bars, was completed with Zen Black or Zen Blue software (Zeiss). Primary antibodies include: anti-PLEKHA7 (Sigma, HPA038610), anti-p120-catenin (15D2, a kind gift from Dr. Albert Reynolds), anti-α-catenin (Abcam, ab231306), anti-β-catenin (BD Transduction, 610154), anti-E-cadherin (BD Transduction, 610182). Secondary antibodies include goat anti-rabbit IgG Alexa 488 (Thermo, A-11034), goat anti-mouse IgG Alexa 488 (Thermo, A-11029), goat anti-rabbit IgG Alexa 594 (Thermo, A-11037), and goat anti-mouse IgG Alexa 594 (Thermo, A-11032).

Analysis of junctional and cytoplasmic staining of p120-catenin and β-catenin staining was performed using Fiji (Fiji is Just Image J, (23)) on maximum projection intensity images. Regions of interest were drawn to contain areas of cytoplasmic staining and exclude areas of apical or basolateral cadherin-catenin staining. Mean pixel intensity was calculated. Linear regions of interest were drawn for apical AJ staining and mean pixel intensity was calculated. Background pixel intensity measurements were subtracted from each. All cytoplasmic staining was averaged for all the cells in a single image and divided by the average junctional intensity for the cells in the same image. Mean apical junctional staining/cytoplasmic staining was calculated for at least 75 cells per group (a total of 9–11 images) for p120-catenin and β-catenin.

Western Blot:

Cells were plated to confluence (Caco2, SUM149) or high density (SUM190, according to manufacturer). Before lysis, cells were rinsed with PBS and lysed with one of the following buffers: RIPA buffer (150 mM NaCl, 50 mM Tris pH 7.4, 0.5% deoxycholic acid, 0.1% SDS, 1% NP-40), Triton-X 100-based buffer (150 mM NaCl, 2 mM EDTA, 25 mM Tris pH 7.4, 0.5% Triton-X 100), or 2X Laemmli sample buffer. For RIPA and Triton-X 100 buffers, 1X protease (Halt's protease inhibitor cocktail, Pierce) and phosphatase (Halt phosphatase inhibitor cocktail, Fisher) inhibitors were added. Lysis with RIPA and Triton-X 100-based buffers was completed on ice. Cells were scraped and lysates passed through a blunt end needle and centrifuged at 4 °C. Protein was quantified using the Pierce BCA Protein Assay (ThermoFisher

Scientific). For lysis with 2X Laemmli sample buffer, cells were scraped and lysates passed through a 25G needle. Protein was quantified using the *RC DC* Protein Assay (Biorad). Before loading, lysates generated from RIPA or Triton-X 100-based buffers were brought to a final concentration of 2X Laemmli sample buffer and boiled for 5 minutes. Samples were separated using 8 or 12% SDS-PAGE gels and transferred to nitrocellulose membranes. Membranes were blocked with 3–5% milk/TBST or 3–5% BSA/TBST and incubated overnight with primary antibodies. Membranes were washed 3 times with TBST, incubated for one hour with secondary antibody, washed 3 times with TBST and incubated with ECL (GE Healthcare). Membranes were imaged onto autoradiography film (Genesee).

Primary antibodies include: anti-PLEKHA7 (Sigma, HPA038610), anti-GAPDH (Cell Signaling, 2118), anti-p120-catenin (15D2, a kind gift from Dr. Albert Reynolds at Vanderbilt University), anti-α-catenin (Sigma, C2081), anti-β-catenin (Sigma, C2206), and anti-E-cadherin (Cell Signaling, 3195). Secondary antibodies include donkey anti-rabbit igG-HRP (Jackson ImmunoResearch, 711-035-152) and donkey anti-mouse IgG-HRP (Jackson ImmunoResearch, 715-035-150).

Matrigel culture:

8-chamber slides (LabTek II) were coated with growth factor reduced Matrigel (BD) and allowed to solidify. 2,500 cells per well were suspended in 2% growth-factor reduced Matrigel and plated. Colonies/spheres formed for approximately two weeks, with regular media changes every 2–3 days. Images were taken using an AMG EVOS digital inverted microscope and number of spheres was counted for each well.

Sphere Compaction:

2,500 cells per well were plated in 96-well round bottom ultra-low attachment plates (Corning). Images were taken at 4X using an AMG EVOS digital inverted microscope at the indicated time points. Images were analyzed in Fiji (23) after conversion to 8 bit images. The threshold was adjusted to include only cells and the area was measured using the measurement tool in Fiji. A representative sample is analyzed and presented. Average area was calculated for 15–18 spheres per group, depending on the time point.

Cell Lines:

The Caco2 cell line was acquired from ATCC. SUM149 and SUM190 cell lines were acquired from Asterand Bioscience (now BIOIVT). All cell lines tested negative for mycoplasma contamination (MycoAlert Mycoplasm detection kit, Lonza AMAXA). Caco2 cells were grown in MEM Eagle with Earle's salts and L-glutamine (Corning) with 10% fetal bovine serum (Gibco), 1X MEM nonessential amino acids (Corning) and 1 nM sodium pyruvate (Gibco). SUM149 and SUM190 cells were grown according to BioIVT instructions. Specifically, SUM149 cells were grown in Ham's F-12 (Gibco) supplemented with 5% heat-inactivated fetal bovine serum (Gibco), 10 mM HEPES (Lonza), 1ug/ml hydrocortisone (Sigma), and 5ug/ml insulin (Sigma). SUM190 cells were grown in Ham's-F-12 (Gibco) supplemented with 1 g/L bovine serum albumin (Sigma), 5 mM ethanolamine (Sigma), 10 mM HEPES (Lonza), 1ug/ml hydrocortisone (Sigma), 5ug/ml insulin (Sigma), 8.7 ng/ml sodium selenite (Sigma), 5ug/ml apo-transferrin (Sigma), and

6.7 ng/ml triiodo-L-thyronine (T3) (Sigma). At time of culturing, a final concentration of 2% heat-inactivated fetal bovine serum (Gibco) was added to media for culturing SUM190 cells.

MTT assay:

2,500 cells/well were plated in flat-bottom 96 well microplates (Fisher). At 24 hours and every 24 hours thereafter, the MTT (Thiazolyl Blue Tetrazolium Bromide) cell viability assay was performed as follows: Fresh media was added to cells followed by addition of 0.83 mg/ml MTT reagent, dissolved in PBS. Reaction proceeded for exactly one hour and was stopped by addition of DMSO. Absorbance was read at 550 nm using a Flexstation 3 Spectrophotometer.

Drug treatment:

2,500 cells/well were plated in round-bottom ultra-low attachment 96 well microplates (Corning) with Microclime lid (Labcyte, Fisher). At 18 hours, doxorubicin was added at indicated concentrations and cells were incubated for an additional 72 hours. Cellular ATP was assessed using the Cell Titer Glo assay (Promega). For this assay, an equal volume of Cell Titer Glo Reagent was added to wells containing cell spheres. The plate was shaken at 55 rpm for 5 minutes and the entire volume was transferred to an opaque plate for reading. Luminescence was read on a Veritas microplate luminometer. ATP content was calculated based on a standard ATP curve. Doxorubicin was obtained from The Mayo Clinic Pharmacy in Jacksonville, FL.

Dual Luciferase Reporter Assay:

SUM149 LZRS ms neo or SUM149 LZRS PLEKHA7 cells were plated to 40–50% confluence and transfected with TopFlash and Renilla-TK, or FopFlash and Renilla Tk reporter plasmids using jetPRIME DNA transfection reagent (Genesee Scientific), according to manufacturer's instructions. Cells were lysed using passive lysis buffer provided in the Dual-Luciferase Reporter Assay system (Promega) and the dual luciferase reporter assay was performed according to manufacturer's instructions. Luciferase signal was read on a Veritas microplate luminometer. TopFlash and FopFlash luciferase signals were normalized by Tk Renilla signal. Further analysis was performed by normalizing TopFlash signal by FopFlash signal.

Animal experiments:

All animal experiments were reviewed and approved by the Institutional Animal Care and Use Committee (IACUC) at Mayo Clinic. All experiments and procedures adhered to the guidelines approved by IACUC. NOD/SCID mice ages 8–10 weeks old were obtained from Jackson laboratories. SUM149 cells tested negative for Ectromelia, LCMV, LDEV, MHV, MPV, MVM, *Mycoplasma pulmonis, Mycoplasma sp*, Polyoma, and TMEV (IDEXX BioResearch). Animals were injected into the 4th mammary fat pad with 1 × 10e5 SUM149 LZRS control (9 mice) or SUM149 LZRS PLEKHA7 cells (8 mice) mixed with Matrigel (BD Transduction Lab) at 1:1. All cells also expressed a luciferase reporter plasmid. Animals were checked daily Monday-Friday for any signs of distress or excessive tumor burden. Tumor volume was measured weekly using a caliper. Luciferase signal was measured weekly using Caliper Life Sciences IVIS imaging

system. One control mouse died unexpectedly during the course of the study and was excluded. After 8 weeks, mice were sacrificed and the tumor was collected and fixed in formalin. Prior to fixation, tumor volume and weight were measured using caliper and microscale, respectively. Two mice in the control group were excluded due to lack of tumor formation (no tumor was visually observed or palpable, and no tumor cells were found by immunohistochemistry of tissue taken from the mammary fat pad).

Immunohistochemistry – ethics statements:

All of the IBC patient samples were originally obtained under the 09-001909 and 08-004581 protocols approved by the Mayo Clinic Institutional Review Board. All patients were consented for tissue collection intended for research purposes. Patient tissue samples were de-identified. Utilization of paraffin-embedded tissue samples for the current research study was performed under the 675-05 protocol, also approved by the Mayo Clinic Institutional Review Board. The Mayo Clinic Institutional Review Board deemed the experiments proposed and performed herein as minimal risk and did not require further consent. A summary of cellular morphology and PLEKHA7 expression is included in Supplementary Table 1.

Immunohistochemistry:

Tissue slides were deparaffinized in xylene and rehydrated with ethanol. Antigen retrieval was performed according to the manufacturer protocol (DAKO) with citrate buffer pH 6.0 (PLEKHA7, Ki67, Snail) or EDTA pH 9.0 (Cyclin D1, c-Myc). Slides were incubated with primary antibody for 1 hour, rinsed with TBST, followed by incubation with secondary antibody for 30 minutes and additional wash with TBST. To stain nuclei, slides were incubated with 3, 3’-diaminobenzidine (DAB) (DAKO) followed by Gills I hematoxylin. Primary antibodies include PLEKHA7 (Sigma, HPA038610), Cyclin D1 (Cell Signaling, 2978), Snail (Cell Signaling, 3879), c-Myc (Abcam, ab32072) and Ki67 (DAKO, M7240).

Slides were scanned using Aperio ScanScope XT (Leica) and viewed using Aperio eSlideManager 12.4.2.5010 and Aperio ImageScope 64 v12.4.2.7000 (Leica). Images were extracted for analysis using Aperio ImageScope 64 v12.4.2.7000 (Leica).

PLEKHA7 staining was analyzed by an independent pathologist. Sixteen samples were excluded due to either lack of staining on internal controls or very few tumor cells found on the slide. IBC tumor samples contained solid and/or glandular cellular patterns based on H&E and PLEKHA7 immunohistochemistry. Each tumor sample was characterized based on the percentage of solid or glandular pattern. The percentage of PLEKHA7 expression and localization was then determined for each cellular pattern. PLEKHA7 staining had the following patterns: 1) normal/apical membrane, 2) lost, 3) cytoplasmic, 4) basal.

For presentation of the data, an average of the percent of PLEKHA7 expression for each of the above four staining patterns was calculated, for either solid or glandular cellular patterns. In the solid areas, the total PLEKHA7 staining add up to 106%, due to some tumor cells demonstrating both a cytoplasmic and basal staining.

To quantify Ki-67, Cyclin D1, Snail, and c-Myc staining of xenograft samples, 5–8 representative and randomly dispersed images of 500 × 500 arbitrary units were captured from each sample using Aperio ImageScope 64 v12.4.2.7000 (Leica). Total nuclei and Ki67, Cyclin D1, Snail or c-Myc positive nuclei were counted in Adobe Photoshop cc 2018 using the counting tool. Ki67, Cyclin D1, Snail or c-Myc positivity was expressed as a fraction of total nuclei and an average from the images was taken for each sample.

Statistical Methods:
Comparisons between control and PLEKHA7 groups were performed using a two-sample t-test. For doxorubicin treatment, a regression model was fit with ATP content as the outcome and group (control/PLEKHA7), doxorubicin dose, and the group by doxorubicin dose interaction as independent variables to determine if the group effect was dependent on dose. Groups were then compared at each dose level using a two-sample t-test. P-values < 0.05 were considered statistically significant.

Results

To start assessing the role of PLEKHA7 in IBC, we determined its expression pattern by immunohistochemistry (IHC) in IBC patient samples. Archival surgical pathology material from 62 patients with a diagnosis of IBC was recovered from the Institutional Tissue Registry from Mayo Clinic Minnesota, Florida, and Arizona campuses and evaluated for adequacy. Sixteen samples were excluded from analysis either due to lack of appropriate tissue (e.g. small representation of neoplastic population) or due to IHC technical issues (e.g. loss of neoplastic population on IHC slides, or failure of IHC staining, as was shown by lack of staining in normal ducts that served as our internal control). Interpretation of hematoxylin and eosin (H&E) and IHC slides was performed by an independent pathologist. Two main morphological patterns were observed: solid and glandular. The predominant pattern of growth was solid, with sparse glandular formations (see Supplemental Fig. 1 for examples). Five tumors demonstrated only solid pattern of growth with no glandular formations. Tumors were divided into predominantly solid (75–100% of tumor exhibits solid pattern of growth), solid (25–74% of tumor exhibits solid pattern of growth), and sparsely solid (0–24% of tumor exhibits solid pattern of growth). The distribution of IBC samples based on the predominance of the solid pattern of growth is displayed in Fig. 1A. Tumors were also categorized based on the percentage of glandular pattern of growth into five categories: 0%, 1–5%, 6–25%, 26–50%, and 51–100%.The distribution of IBC samples based on the glandular pattern of growth is displayed in Fig. 1B.

PLEKHA7 expression was distinct between the solid and glandular patterns. For each morphological pattern, the average PLEKHA7 staining pattern across all tumor samples was calculated and categorized based on localization (apical, lost, cytoplasmic, or basal). In solid areas, PLEKHA7 was lost in 56.4%, while cytoplasmic pattern was observed in 26.4% and localized to the basal membrane in 24.1% across all IBC tumor samples (See Fig. 1C). Apical staining was not observed in solid areas of the tumor. In contrast, PLEKHA7 staining in glandular areas was either lost (68.6%) or apical (31.4%) (See Fig. 1D). Examples of PLEKHA7 staining for each location are shown in Fig. 1E-I. For complete breakdown and analysis of PLEKHA7 expression in IBC samples, see Supplemental Table 1. It is notable that PLEKHA7

must properly localize to the apical AJs to maintain its tumor suppressing function (19). Therefore, we anticipate that PLEKHA7 would not be functional in the overwhelming majority of these patient tumors.

To further interrogate the function of PLEKHA7 in IBC, we utilized two frequently used cell line models: SUM149 and SUM190. SUM149 cells belong to the triple negative basal molecular subtype, while SUM190 to the hormone receptor negative, erbB2/Her2 positive molecular subtype. Western blot experiments indicated that both SUM149 and SUM190 cell lines express very low levels of PLEKHA7 protein compared to Caco2 cells, an often utilized epithelial model for studying the AJs (see Fig. 1J). Collectively, these data suggest a consistent loss of functional PLEKHA7 in IBC, despite normal to high expression of p120 and E-cadherin (Fig. 1J and previous studies) (5, 17).

Next, we used viral transduction to examine the effects of PLEKHA7 re-expression in SUM149 cells. We found that exogenously expressed PLEKHA7 localizes to and strengthens the AJs, as evidenced by increased junctional accumulation of p120, E-cadherin, α-catenin, and β-catenin (see Fig. 2A-B). This junctional strengthening is similar to previous reports (19, 20, 24). Notably, PLEKHA7 re-expression altered the location, but not the overall levels of junctional proteins (see Fig. 2C), also consistent with previous publications (19, 20). In agreement, we observed decreased cytoplasmic localization of p120 and β-catenin in PLEKHA7-expressing cells (see Fig. 2B).

p120 regulates the activities of RhoGTPases, including RhoA, Rac1, and Cdc42 (25–27), as well as RhoGEFs and RhoGAPs (26, 28). The ability of p120 to regulate RhoGTPase signaling is thought to be regulated by p120's junctional vs. cytoplasmic localization, and is essential for EGFR, HER2, Rac1, and Src-mediated induction of tumorigenesis (29–31). Depletion of p120 suppressed the growth and emboli formation of SUM149 cells in vitro, suggesting an important role for p120 in IBC (17). In this study, we did not explore further the possibility that 1) p120 promotes tumor growth by regulating RhoGTPase signaling in SUM149 cells, or that 2) restoring PLEKHA7 decreases the capacity of p120 to function in this manner.

As increased cytoplasmic β-catenin could lead to increased nuclear signaling, we tested for altered activity in the Wnt/β-catenin pathway using the dual luciferase reporter assay (Fig. 2D). Although TopFlash activity is reduced in PLEKHA7-SUM149 compared to control, we did not see consistent changes in activity when normalized by the FopFlash reporter (Fig. 2D). Therefore, while PLEKHA7 expression increases the junctional localization of β-catenin, it does not affect Wnt/β-catenin nuclear signaling under these conditions in SUM149 cells.

To test the hypothesis that PLEKHA7 loss in IBC promotes a more aggressive phenotype, we next examined whether restoring PLEKHA7 to the apical AJs suppresses cell growth. Under 2D culture conditions, PLEKHA7-expressing SUM149 cells exhibited reduced proliferative capacity, compared to SUM149 cells infected with control virus (Supplemental Fig. 2). Further, when PLEKHA7-expressing SUM149 cells were plated on Matrigel, they formed fewer and smaller colonies compared to control SUM149 cells (see Fig. 3A-B). IBC patients frequently demonstrate tumor emboli in the dermal lymphatics, and spheroid formation under ultra-low attachment conditions has been used as a model of

IBC tumor emboli (7). SUM149 cells infected with control virus rapidly formed compact spheres when grown in suspension. In contrast, PLEKHA7-expressing SUM149 were more loosely connected and less compacted than control SUM149 cells (see Fig. 3C-D). Interestingly, the ability of IBC cells to form compact spheroids has been correlated directly to their tumorigenic potential (7). We also hypothesized that the less compacted spheres would be more vulnerable to chemotherapy treatment. To test this, we determined the sensitivity of control and PLEKHA7-expressing SUM149 spheres to doxorubicin, a standard neoadjuvant chemotherapy used in IBC treatment. Notably, after 72 hours of treatment, PLEKHA7-SUM149 spheres were significantly less viable than control-SUM149 spheres in response to doxorubicin treatment, particularly at the highest doses (10uM) (see Fig. 3E).

Our *in vitro* and IHC data argued that PLEKHA7 acts as a tumor suppressor and is frequently misregulated in IBC. Next we tested whether restoring PLEKHA7 expression in SUM149 cells would decrease tumor formation or growth in an animal model. SUM149 cells reliably form tumors in xenograft models when injected orthotopically (17, 32). PLEKHA7-expressing SUM149 cells or control SUM149 cells were injected into the 4th mammary fat pad of NOD/SCID mice and mice were monitored for 8 weeks for the presence and size of tumors formed. Mouse body weight changes were not observed in either group. After 8-weeks, mice were sacrificed and tumors were obtained for IHC. As shown in Fig. 4A and 4B, tumors in the PLEKHA7-expressing SUM149 mice were smaller and less proliferative than control. Importantly, IHC analysis revealed that PLEKHA7 expression was commonly misregulated in the PLEKHA7-expressing tumors. After 8 weeks, we found that most of the PLEKHA7-tumors had lost significant expression of PLEKHA7, retaining between 15–55% PLEKHA7 depending on the mouse. Furthermore, we frequently observed cytoplasmic PLEKHA7 staining, with only approximately 10–25% junctional PLEKHA7 remaining in most tumors. An example is shown in Fig. 4C. This indicates a negative selection of PLEKHA7-expressing tumor cells. Accordingly, when we quantified tumors for changes in Snail, Myc, and Cyclin D1, proteins that have been previously shown to be suppressed by PLEKHA7 function in Caco2 cells (19), we observed a trend towards reduced expression in PLEKHA7-SUM149 tumors that did not reach significance (see Supplemental Fig. 4A-C). We hypothesize that the tumor suppressive effects observed with PLEKHA7 expression in SUM149 xenografts occurred early in tumor formation. This early-effect hampered tumor growth sufficiently enough to observe overall differences in tumor between groups. However, PLEKHA7-positive tumors escaped these suppressive effects by deregulating ectopically expressed PLEKHA7 throughout the 8-week course of the experiment.

Discussion

Understanding the molecular alterations contributing to the uniquely aggressive phenotype and clinical course of IBC has proven quite challenging. In this study, we tested the hypothesis that IBC is, in part, driven by the imbalance of basolateral to apical cadherin-catenin-complex activity. Specifically, we tested and demonstrated that restoration of apical complex protein PLEKHA7 inhibits the aggressive nature of IBC.

E-cadherin is considered a tumor suppressor, and loss of E-cadherin (CDH1) expression is a cardinal feature of invasive lobular carcinoma of the breast (33, 34). Nonetheless, strong expression of E-cadherin is consistently observed in IBC primary tumors and tumor emboli in the dermal lymphatics (5). Evidence in animal and in-vitro models suggests a causative role for E-cadherin in maintaining cohesion of tumor emboli and tumor growth (7, 17). Silvera et al also identified a tumor-promoting and emboli-forming role for p120 in IBC cell line and xenograft models (17), which was attributed to its ability to promote the stability and junctional retention of E-cadherin. There is now increasing evidence that in several tumor types, including IBC, E-cadherin complexes can promote tumor growth and metastasis (35, 36).

Recent work from our lab determined distinct functional roles for apical vs basolateral cadherin-catenin complexes. Basolateral cadherin-catenin complexes promote AIG and expression of pro-tumorigenic factors. Apical cadherin-catenin complexes suppress expression of these factors and inhibit AIG through a mechanism that depends on PLEKHA7 (19). We postulated that the aggressive nature of IBC is mediated by an imbalance between the tumor promoting basolateral and the tumor suppressing apical cadherin-catenin complexes. We tested this hypothesis by focusing on the expression and function of PLEKHA7 in IBC. We find that PLEKHA7 expression is largely not apical in IBC tumors, indicating a loss of tumor suppressing function in this disease. This is very consistent with previous reports that PLEKHA7 is lost or mislocalized in invasive ductal carcinoma (19, 37, 38). One group found that PLEKHA7 is primarily cytoplasmic in invasive lobular carcinoma, presumably due to E-cadherin loss (37), particularly in comparison to invasive ductal carcinoma, where little-to-no expression of PLEKHA7 is observed. Importantly, the tumor suppressing function of PLEKHA7 depends on apical junctional localization (19), and this is disrupted in IBC patient tumors. Whether mislocalization of PLEKHA7 to the cytoplasm or the basal membrane confers additional functions – either oncogenic or tumor-suppressive – is currently unclear.

Both IBC cell lines tested revealed very low PLEKHA7 expression. Ectopic expression of PLEKHA7 was largely junctional and resulted in strong recruitment of cadherin-catenin complex proteins to PLEKHA7-positive junctions, in agreement with previous studies (19, 20, 24). Interestingly, PLEKHA7 re-expression redistributed p120 and β-catenin away from the cytoplasm and into the apical AJ. While not tested directly here, this may have functional consequences as cytoplasmic localization of p120 can suppress RhoA activity (Reviewed in (39)). We did not, however, observe consistent changes in β-catenin-nuclear activity between PLEKHA7-expressing or control-SUM149 cells. Increased junctional and decreased cytoplasmic β-catenin localization upon PLEKHA7 expression was also observed in an ovarian cancer model, but alterations to β-catenin-nuclear activity were not tested in that study (40).

Consistent with the hypothesis that PLEKHA7 acts as a tumor suppressor that is commonly lost in IBC, its re-expression in an IBC cell line significantly inhibited cell growth, both in 2D and particularly in 3D culture. Our data also indicates that PLEKHA7 re-expression suppresses both the number and size of SUM149 colonies on Matrigel. We did not test the mechanism by which PLEKHA7 executes these tumor-suppressor roles in IBC. Previous studies determined that PLEKHA7 recruits the RNAi machinery to the apical AJs to promote the maturation of miRNAs and their association with an apically localized RNA-

induced silencing complex (RISC) (19, 24). This function of PLEKHA7 suppressed expression of pro-tumor promoting proteins and inhibited AIG. Recent work in colon cancer patient samples demonstrated concomitant dysfunction of PLEKHA7 and the RNAi machinery at the apical AJs during colon cancer progression (41). When PLEKHA7 was restored in colon cancer cell lines, the RNAi machinery was also restored to apical AJ, and PLEKHA7-expressing xenografts showed reduced tumor burden (41).

We cannot exclude the possibility that other mechanisms contribute to the tumor suppressive function of PLEKHA7 in IBC, including inhibiting p120 signaling, or suppressing of E-cadherin/EGFR signaling (40). In certain ovarian epithelial cancer lines, E-cadherin has been shown to promote EGFR signaling, and this is suppressed by expression of PLEKHA7 (40). The ability of E-cadherin to promote EGFR signaling in IBC is unexplored, but EGFR expression has been observed in approximately 30% of IBC samples (42). In that study, IBC patients with EGFR-positive tumors had worse overall survival (42).

Re-expression of PLEKHA7 suppressed in-vitro spheroid compaction in 3D culture. Increased cohesion of tumor emboli is a key characteristic of IBC. We observed that suppression of sphere compaction in PLEKHA7-expressing cells led to decreased survival after treatment with doxorubicin, a standard neoadjuvant chemotherapy used in IBC treatment. In orthotopic xenograft models, re-expression of PLEKHA7 slowed tumor growth, leading to decreased tumor volume. Notably, by the end of our 8-week study, we also observed that the majority of PLEKHA7-expressing tumors had bypassed PLEKHA7 tumor-suppression by losing PLEKHA7 or causing a cytoplasmic localization. This suggests the existence of selective pressure in tumor cells to lose apical PLEKHA7 expression.

Altogether, our data is consistent with an important tumor suppressor function for PLEKHA7 in IBC. While the mechanisms of its loss or mislocalization away from the apical AJs are still unclear, PLEKHA7 dysfunction is almost universal in IBC patient samples. Re-expression of PLEKHA7 restores apical AJs and suppresses tumor growth in vitro and in vivo. These data suggest a more nuanced understanding of the role that the cadherin-catenin complex plays in promoting IBC. Specifically, our data indicate that IBC growth and emboli formation are promoted by the abundance of basolateral cadherin-catenin complexes and the lack of tumor-suppressive apical cadherin-catenin complexes.

Conclusions

Inflammatory breast cancers are characterized by robust expression of E-cadherin and other members of the cadherin-catenin axis, including p120. These proteins are thought to promote IBC survival and metastasis by maintaining cohesive, viable tumor emboli in the dermal lymphatics. We provide new insights into this view by demonstrating that the apical adherens junction complex, characterized by the presence of PLEKHA7, is disrupted in IBC. In the absence of sufficient negative regulation by the apical complex, we anticipate the abundant basolateral cadherin-catenin complex promotes the aggressive nature of IBC tumors. In support, our data shows that restoring apical complex activity, via PLEKHA7, is sufficient to suppress IBC tumor growth in vitro and in-vivo.

Abbreviations

AIG: Anchorage independent growth

AJ: Adherens junction

IACUC: Institutional Animal Care and Use Committee

IBC: Inflammatory Breast Cancer

IHC: Immunohistochemistry

IRES: Internal ribosomal entry site

miRNA: micro-RNA

RISC: RNA-induced silencing complex

RNAi: RNA-interference

Declarations

Ethics Declarations

All of the inflammatory breast cancer patient samples were originally obtained under the 09-001909 and 08-004581 protocols approved by the Mayo Clinic Institutional Review Board. All patients were consented for tissue collection intended for research purposes. Patient tissue samples were de-identified. Utilization of paraffin-embedded tissue samples for the current research study was performed under the 675-05 protocol, also approved by the Mayo Clinic Institutional Review Board. The Mayo Clinic Institutional Review Board deemed the experiments proposed and performed herein as minimal risk and did not require further consent.
The animal study performed herein was reviewed and approved by Mayo Clinic's Institutional Animal Care and Use Committee (IACUC). Researchers adhered to the approved protocol and guidelines.

Consent for publication:

Not applicable.

Availability of data and materials:

Tumor sample datasets analyzed during this study are included in this published article and its supplementary files. Any additional data analyzed during this study are available upon contact to the corresponding author.

Competing interests:

The authors have no competing interests.

Funding:

Studies in this project were supported by a developmental research award to PZA from NCI P50 CA11620, and by R01 NS101721-01A1 (PZA).

Authors contributions:

LJP, AK and PZA generated the intellectual ideas of the study. LJP conducted the experiments for all presented data excluding Figure 3A-B. AK completed the experiments for data presented in Figure 3A-B. LJP wrote the manuscript. RWF and MTH supported the animal study. SS performed all the analysis of the IBC patient samples presented in Figure 1. PD performed the statistical analysis for the animal study and the doxorubicin drug treatment (Figure 3D and 4A). AN, ITC, and SSS were integral in identifying IBC patients and acquiring patient samples for the study.

Acknowledgements:

The authors thank Dr. Albert Reynolds and Dr. Aubrey Thompson for their generous sharing of plasmids. The authors thank Brandy Edenfield and Dr. Laura Lewis-Tuffin for their technical support with immunohistochemistry and imaging, respectively. The authors also thank Dr. Wan-Hsin Lin for excellent suggestions throughout the study.

References

1. Hance KW, Anderson WF, Devesa SS, Young HA, Levine PH. Trends in inflammatory breast carcinoma incidence and survival: the surveillance, epidemiology, and end results program at the National Cancer Institute. J Natl Cancer Inst. 2005;97(13):966-75.
2. Anderson WF, Schairer C, Chen BE, Hance KW, Levine PH. Epidemiology of inflammatory breast cancer (IBC). Breast Dis. 2005;22:9-23.
3. Dawood S, Merajver SD, Viens P, Vermeulen PB, Swain SM, Buchholz TA, et al. International expert panel on inflammatory breast cancer: consensus statement for standardized diagnosis and treatment. Ann Oncol. 2011;22(3):515-23.
4. Bertucci F, Finetti P, Vermeulen P, Van Dam P, Dirix L, Birnbaum D, et al. Genomic profiling of inflammatory breast cancer: a review. Breast. 2014;23(5):538-45.
5. Kleer CG, van Golen KL, Braun T, Merajver SD. Persistent E-cadherin expression in inflammatory breast cancer. Mod Pathol. 2001;14(5):458-64.
6. Alpaugh ML, Tomlinson JS, Shao ZM, Barsky SH. A novel human xenograft model of inflammatory breast cancer. Cancer Res. 1999;59(20):5079-84.
7. Tomlinson JS, Alpaugh ML, Barsky SH. An intact overexpressed E-cadherin/alpha,beta-catenin axis characterizes the lymphovascular emboli of inflammatory breast carcinoma. Cancer Res.

2001;61(13):5231-41.

8. Meng W, Takeichi M. Adherens junction: molecular architecture and regulation. Cold Spring Harb Perspect Biol. 2009;1(6):a002899.
9. Ireton RC, Davis MA, van Hengel J, Mariner DJ, Barnes K, Thoreson MA, et al. A novel role for p120 catenin in E-cadherin function. J Cell Biol. 2002;159(3):465-76.
10. Davis MA, Ireton RC, Reynolds AB. A core function for p120-catenin in cadherin turnover. J Cell Biol. 2003;163(3):525-34.
11. Bruser L, Bogdan S. Adherens Junctions on the Move-Membrane Trafficking of E-Cadherin. Cold Spring Harb Perspect Biol. 2017;9(3).
12. Ishiyama N, Lee SH, Liu S, Li GY, Smith MJ, Reichardt LF, et al. Dynamic and static interactions between p120 catenin and E-cadherin regulate the stability of cell-cell adhesion. Cell. 2010;141(1):117-28.
13. Fujita Y, Krause G, Scheffner M, Zechner D, Leddy HE, Behrens J, et al. Hakai, a c-Cbl-like protein, ubiquitinates and induces endocytosis of the E-cadherin complex. Nat Cell Biol. 2002;4(3):222-31.
14. Marambaud P, Shioi J, Serban G, Georgakopoulos A, Sarner S, Nagy V, et al. A presenilin-1/gamma-secretase cleavage releases the E-cadherin intracellular domain and regulates disassembly of adherens junctions. EMBO J. 2002;21(8):1948-56.
15. Miyashita Y, Ozawa M. Increased internalization of p120-uncoupled E-cadherin and a requirement for a dileucine motif in the cytoplasmic domain for endocytosis of the protein. J Biol Chem. 2007;282(15):11540-8.
16. Yap AS, Niessen CM, Gumbiner BM. The juxtamembrane region of the cadherin cytoplasmic tail supports lateral clustering, adhesive strengthening, and interaction with p120ctn. J Cell Biol. 1998;141(3):779-89.
17. Silvera D, Arju R, Darvishian F, Levine PH, Zolfaghari L, Goldberg J, et al. Essential role for eIF4GI overexpression in the pathogenesis of inflammatory breast cancer. Nat Cell Biol. 2009;11(7):903-8.
18. Takeichi M. Dynamic contacts: rearranging adherens junctions to drive epithelial remodelling. Nat Rev Mol Cell Biol. 2014;15(6):397-410.
19. Kourtidis A, Ngok SP, Pulimeno P, Feathers RW, Carpio LR, Baker TR, et al. Distinct E-cadherin-based complexes regulate cell behaviour through miRNA processing or Src and p120 catenin activity. Nat Cell Biol. 2015;17(9):1145-57.
20. Meng W, Mushika Y, Ichii T, Takeichi M. Anchorage of microtubule minus ends to adherens junctions regulates epithelial cell-cell contacts. Cell. 2008;135(5):948-59.
21. Pulimeno P, Bauer C, Stutz J, Citi S. PLEKHA7 is an adherens junction protein with a tissue distribution and subcellular localization distinct from ZO-1 and E-cadherin. PLoS One. 2010;5(8):e12207.
22. Kourtidis A, Necela B, Lin WH, Lu R, Feathers RW, Asmann YW, et al. Cadherin complexes recruit mRNAs and RISC to regulate epithelial cell signaling. J Cell Biol. 2017;216(10):3073-85.

23. Schindelin J, Arganda-Carreras I, Frise E, Kaynig V, Longair M, Pietzsch T, et al. Fiji: an open-source platform for biological-image analysis. Nat Methods. 2012;9(7):676-82.
24. Kourtidis A, Anastasiadis PZ. PLEKHA7 defines an apical junctional complex with cytoskeletal associations and miRNA-mediated growth implications. Cell Cycle. 2016;15(4):498-505.
25. Anastasiadis PZ, Moon SY, Thoreson MA, Mariner DJ, Crawford HC, Zheng Y, et al. Inhibition of RhoA by p120 catenin. Nat Cell Biol. 2000;2(9):637-44.
26. Noren NK, Liu BP, Burridge K, Kreft B. p120 catenin regulates the actin cytoskeleton via Rho family GTPases. J Cell Biol. 2000;150(3):567-80.
27. Grosheva I, Shtutman M, Elbaum M, Bershadsky AD. p120 catenin affects cell motility via modulation of activity of Rho-family GTPases: a link between cell-cell contact formation and regulation of cell locomotion. J Cell Sci. 2001;114(Pt 4):695-707.
28. Wildenberg GA, Dohn MR, Carnahan RH, Davis MA, Lobdell NA, Settleman J, et al. p120-catenin and p190RhoGAP regulate cell-cell adhesion by coordinating antagonism between Rac and Rho. Cell. 2006;127(5):1027-39.
29. Dohn MR, Brown MV, Reynolds AB. An essential role for p120-catenin in Src- and Rac1-mediated anchorage-independent cell growth. The Journal of cell biology. 2009;184(3):437-50.
30. Mariner DJ, Davis MA, Reynolds AB. EGFR signaling to p120-catenin through phosphorylation at Y228. J Cell Sci. 2004;117(Pt 8):1339-50.
31. Johnson E, Seachrist DD, DeLeon-Rodriguez CM, Lozada KL, Miedler J, Abdul-Karim FW, et al. HER2/ErbB2-induced breast cancer cell migration and invasion require p120 catenin activation of Rac1 and Cdc42. The Journal of biological chemistry. 2010;285(38):29491-501.
32. Kleer CG, Zhang Y, Pan Q, van Golen KL, Wu ZF, Livant D, et al. WISP3 is a novel tumor suppressor gene of inflammatory breast cancer. Oncogene. 2002;21(20):3172-80.
33. Moll R, Mitze M, Frixen UH, Birchmeier W. Differential loss of E-cadherin expression in infiltrating ductal and lobular breast carcinomas. Am J Pathol. 1993;143(6):1731-42.
34. Gamallo C, Palacios J, Suarez A, Pizarro A, Navarro P, Quintanilla M, et al. Correlation of E-cadherin expression with differentiation grade and histological type in breast carcinoma. Am J Pathol. 1993;142(4):987-93.
35. Padmanaban V, Krol I, Suhail Y, Szczerba BM, Aceto N, Bader JS, et al. E-cadherin is required for metastasis in multiple models of breast cancer. Nature. 2019;573(7774):439-44.
36. Rodriguez FJ, Lewis-Tuffin LJ, Anastasiadis PZ. E-cadherin's dark side: possible role in tumor progression. Biochim Biophys Acta. 2012;1826(1):23-31.
37. Castellana B, Escuin D, Perez-Olabarria M, Vazquez T, Munoz J, Peiro G, et al. Genetic up-regulation and overexpression of PLEKHA7 differentiates invasive lobular carcinomas from invasive ductal carcinomas. Hum Pathol. 2012;43(11):1902-9.
38. Tille JC, Ho L, Shah J, Seyde O, McKee TA, Citi S. The Expression of the Zonula Adhaerens Protein PLEKHA7 Is Strongly Decreased in High Grade Ductal and Lobular Breast Carcinomas. PLoS One.

2015;10(8):e0135442.
39. Anastasiadis PZ. p120-ctn: A nexus for contextual signaling via Rho GTPases. Biochim Biophys Acta. 2007;1773(1):34-46.
40. Rea K, Roggiani F, De Cecco L, Raspagliesi F, Carcangiu ML, Nair-Menon J, et al. Simultaneous E-cadherin and PLEKHA7 expression negatively affects E-cadherin/EGFR mediated ovarian cancer cell growth. J Exp Clin Cancer Res. 2018;37(1):146.
41. Nair-Menon J, Daulagala AC, Connor DM, Rutledge L, Penix T, Bridges MC, et al. Predominant Distribution of the RNAi Machinery at Apical Adherens Junctions in Colonic Epithelia Is Disrupted in Cancer. Int J Mol Sci. 2020;21(7).
42. Cabioglu N, Gong Y, Islam R, Broglio KR, Sneige N, Sahin A, et al. Expression of growth factor and chemokine receptors: new insights in the biology of inflammatory breast cancer. Ann Oncol. 2007;18(6):1021-9.

Figures

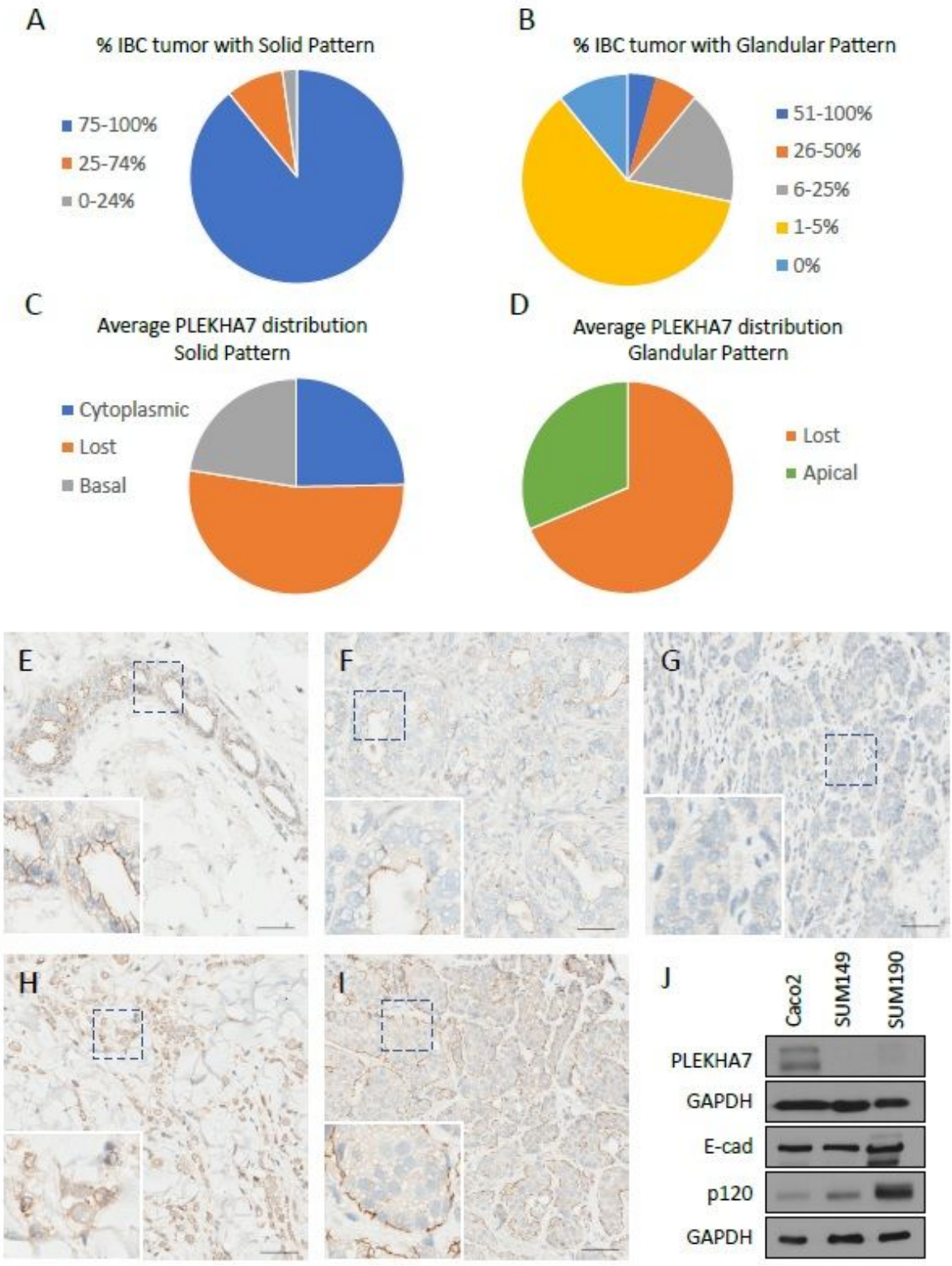

Figure 1

PLEKHA7 expression in IBC patient samples and cell lines. A) Pie chart displaying the number of IBC patient samples demonstrating solid tumor patterns in 0-24% (N=1 tumor), 25-74% (N=4 tumors), or 75-100% (N=41 tumors) of the total tumor. B) Pie chart displaying the number of IBC patient samples demonstrating glandular tumor patterns in 0% (N=5 tumors), 1-5% (N=28 tumors), 6-25% (N=8 tumors), 26-50% (N=3 tumors), or 51-100% (N=2 tumors) of the total tumor. C) Pie chart depicting the average

percentage of PLEKHA7 expression as lost (56.4%), cytoplasmic (26.4%) or basal (24.1%) in the regions of solid tumor from all IBC patient samples. No apical staining of PLEKHA7 was observed in areas of solid tumor. Note that total percentage is 106.9% since some tumor cells demonstrated both a cytoplasmic and basal staining pattern. D) Pie chart depicting the average percentage of PLEKHA7 expression as lost (68.6%) or apical (31.4%) in the regions of glandular tumor from all IBC patient samples. No cytoplasmic or basal staining of PLEKHA7 was observed in areas of glandular tumor. E) Expression of PLEKHA7 by IHC in normal breast tissue. F-I) Examples of expression patterns for PLEKHA7 in IBC patient samples. F) apical staining, G) loss of staining, H) cytoplasmic staining and I) basal staining. J) Expression of PLEKHA7, E-cadherin, and p120-catenin by Western blot.

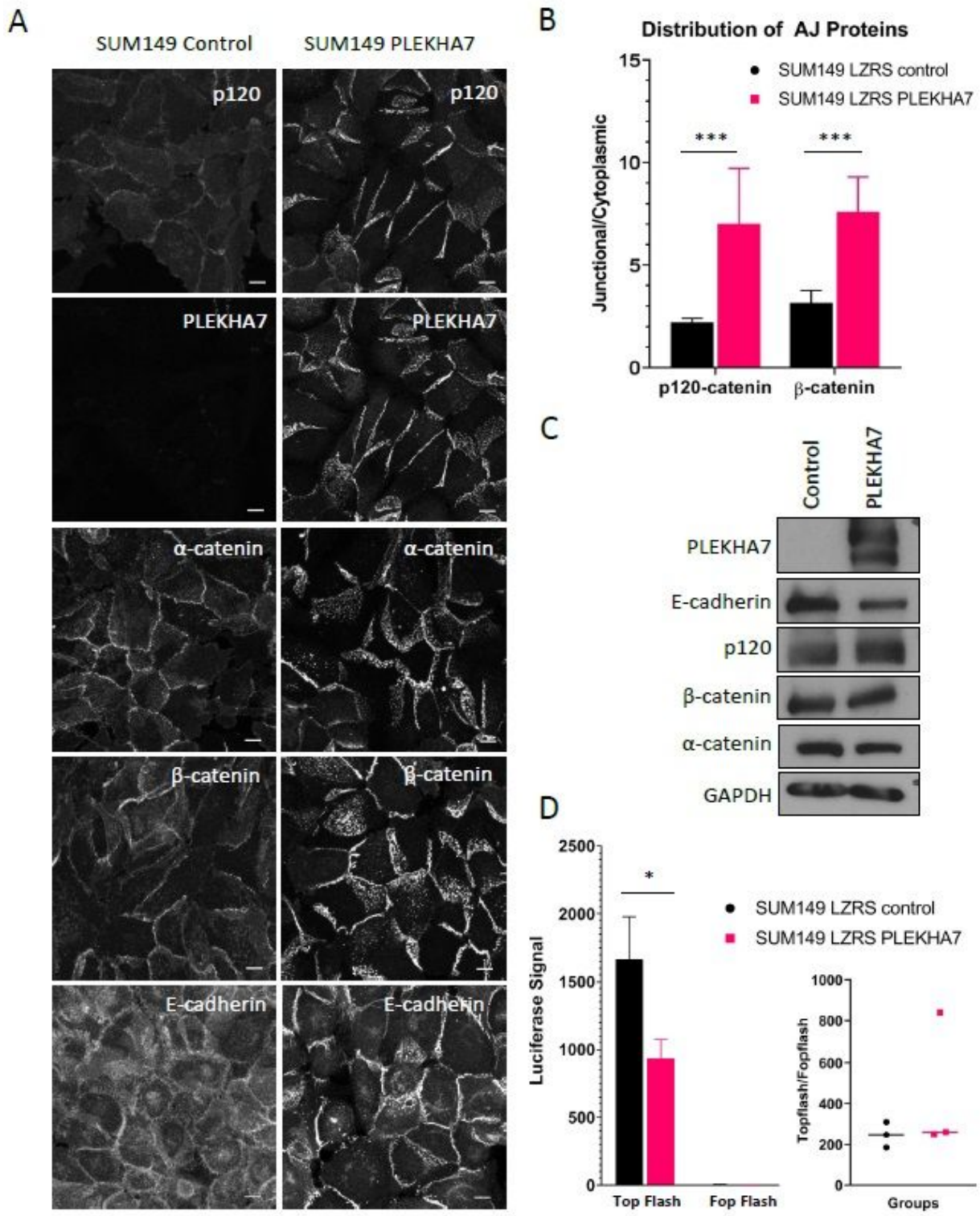

Figure 2

Effect of PLEKHA7 re-expression on SUM149 cell adherens junctions. A) SUM149 cells expressing LZRS ms neo (control) or LZRS PLEKHA7 were grown to confluence and immunofluorescence was performed for E-cadherin, p120-catenin, PLEKHA7, α-catenin or β-catenin. Images were obtained by confocal microscopy. Images are maximum projection intensity. Scale bar is 10μM. B) Intensity of p120-catenin or β-catenin staining is expressed as a ratio of signal at apical AJs to cytoplasmic staining. N>75 cells per

condition per group. ***indicates p<0.001 by Student's t-test (p<0.0001 for both p120-catenin and β-catenin). C) Protein levels of PLEKHA7, E-cadherin, p120-catenin, β-catenin, and α-catenin in SUM149 LZRS ms neo or SUM149 LZRS PLEKHA7 cells were obtained by Western blot. D) A representative graph displaying Wnt/β-catenin signaling in SUM149 LZRS ms neo and SUM149 LZRS PLEKHA7 cell lines using dual luciferase reporter assay. * indicates p<0.05 by Student's t-test (p=0.022).

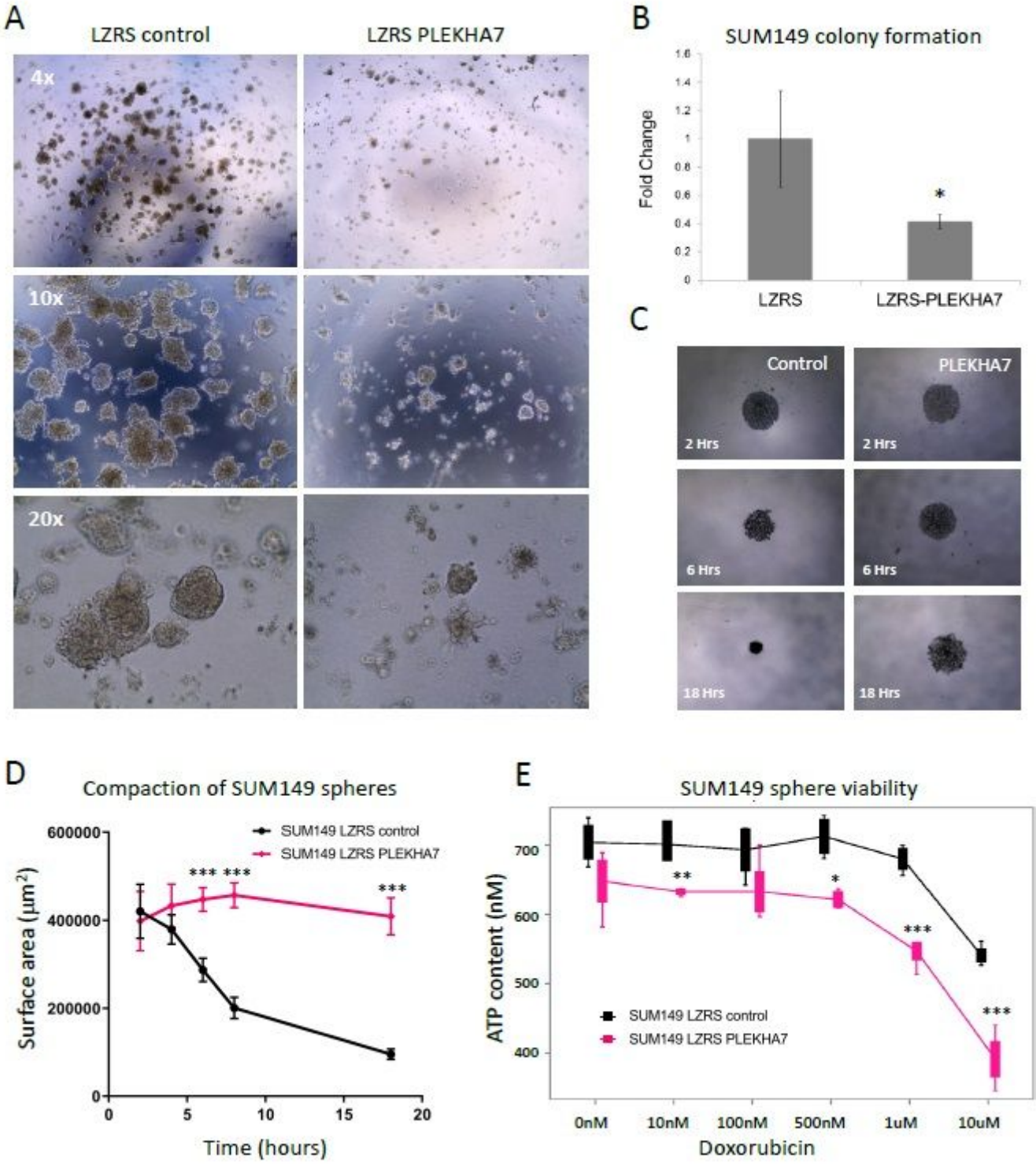

Figure 3

Effects of PLEKHA7 re-expression on SUM149 cell growth and survival in 3D culture. A) SUM149 LZRS ms neo (control) or SUM149 LZRS PLEKHA7 cells were grown in Matrigel for approximately 2 weeks. Representative images at 4X, 10X and 20X magnification are shown. B) Quantification of SUM149 LZRS ms neo or SUM149 LZRS PLEKHA7 colonies from 3A are shown as fold change from SUM149 LZRS ms neo. * indicates $p<0.05$ by Student's t-test. C) Representative images from SUM149 LZRS ms neo or SUM149 LZRS PLEKHA7 suspension cultures undergoing sphere compaction over 18 hours. Images taken at 4X. D) A representative graph of SUM149 LZRS ms neo or SUM149 LZRS PLEKHA7 suspension cultures compacting into spheres over 18 hours under ultra-low attachment conditions. *** indicates $p<0.001$ by Student's t-test ($p<0.0001$). E) A representative graph of ATP content produced by SUM149 LZRS ms neo or SUM149 PLEKHA7 spheres after treatment with various concentrations of doxorubicin for 72 hours. * indicates $p<0.05$ by Student's t-test, ** indicates $p<0.01$ by Student's t-test, *** indicates $p<0.001$ by Student's t-test ($p=0.005$ for 10nm dox, $p=0.092$ for 100nm dox, $p= 0.001$ for 500nm dox, $p=0.0001$ for 1μm dox, and $p=0.0004$ for 10μm dox).

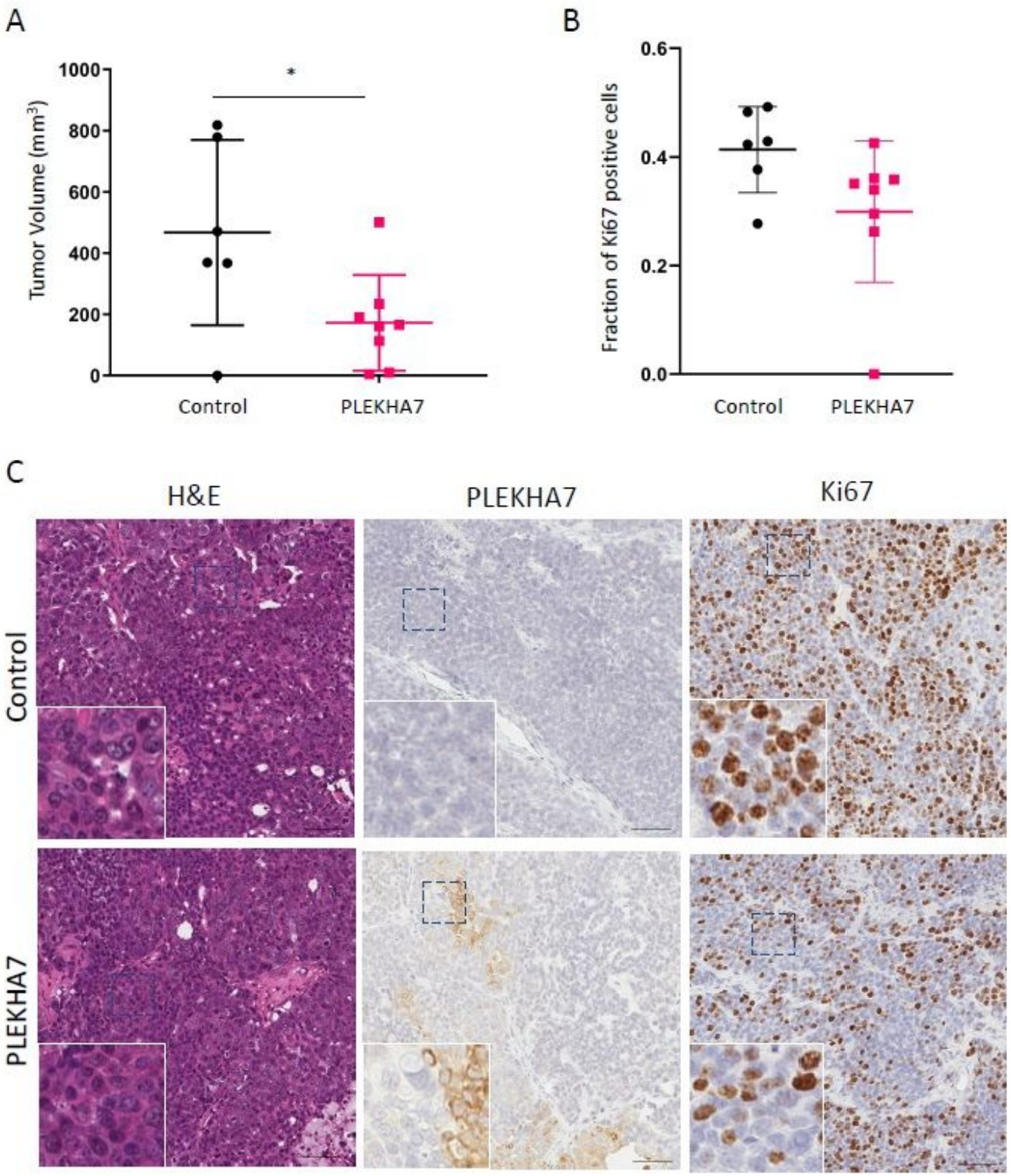

Figure 4

PLEKHA7 effects on SUM149 tumor growth in orthotopic xenografts. A) Tumor volume of xenografts from SUM149 LZRS ms neo (control) or SUM149 LZRS PLEKHA7 cells implanted into the 4th mammary gland of NOD/SCID mice measured at 8-weeks post-implantation. * indicates p=0.034 by student's t-test. n=6 for control group, n= 8 for PLEKHA7 group. B) Fraction of Ki-67 positive cells in tumors from SUM149 LZRS ms neo or SUM149 LZRS PLEKHA7 xenografts at the 8-week end-point. p=0.082 by student's t-test.

n=6 for control group, n= 8 for PLEKHA7 group. C) Representative IHC images from SUM149 LZRS ms neo or SUM149 LZRS PLEKHA7 xenografts for H&E, PLEKHA7, and Ki67. Scale bar represents 100um.

Supplementary Files

This is a list of supplementary files associated with this preprint. Click to download.

- SupplementalTable1.xlsx
- SupplementalFigure1.pdf
- SupplementalFigure2.pdf
- SupplementalFigure3.pdf